PHYSICAL REVIEW B VOLUME 26, NUMBER 2 15 JULY 1982

Influence of the exchange interaction on far-infrared spin-flip resonances in zero-gap $Hg_{1-x}Mn_xSe$

A. Witowski,* K. Pastor,* and J. K. Furdyna
Physics Department, Purdue University, West Lafayette, Indiana 47907
(Received 5 March 1982)

Far-infrared (FIR) magnetotransmission experiments were carried out on the diluted magnetic ("semimagnetic") semiconductor $Hg_{1-x}Mn_xSe$ with $x=0.03$ with the use of an optically pumped FIR laser. Measurements were performed in magnetic fields up to 2.5 T in both Voigt and Faraday geometries, at FIR wavelengths between 96.5 and 170 μm in the temperature range between 1.9 and 6.5 K. We report the observation of the electric-dipole-excited conduction-electron-spin-resonance (EDSR) and combined-resonance transitions. These intraband spin-flip resonances are made possible by the relaxation of the electric-dipole selection rules through the $\vec{k}\cdot\vec{p}$ interaction or inversion asymmetry, in the presence of spin-orbit coupling. Because of the exchange interaction between the conduction electrons and the magnetic moments localized on the Mn^{2+} ions, the spin splitting of the electronic Landau levels is extremely large and is temperature dependent. This manifests itself as a dramatic temperature variation of the positions of EDSR and of the combined resonance. The results of the experiments are analyzed with a numerical fitting procedure using the Pidgeon-Brown model which has been modified to include the effects of the exchange interaction. The analysis yields conduction band and exchange parameters for $Hg_{1-x}Mn_xSe$ of small Mn content.

I. INTRODUCTION

The ternary compound $Hg_{1-x}Mn_xSe$ belongs to the group of so-called diluted magnetic (or "semimagnetic") semiconductors, which are characterized by the presence of a strong spin-spin exchange interaction between the localized magnetic moments of Mn^{2+} and the band electrons.[1] These materials therefore offer a unique opportunity of studying the influence of the exchange interaction on electronic states in semiconductors. As a result of this interaction one expects, for example, extremely large spin splittings of Landau levels, as well as a very strong temperature dependence of this splitting. These effects are particularly pronounced when the Mn content is relatively low (for example, $x<0.06$), i.e., when $Hg_{1-x}Mn_xSe$ is a zero-gap semiconductor.

One of the best experimental methods of investigating the behavior of spin substates of conduction electrons in the presence of magnetic exchange is the far-infrared (FIR) magnetospectroscopy. FIR measurements, however, are particularly difficult in zero-gap $Hg_{1-x}Mn_xSe$ because, just as in the case of pure HgSe, these ternary materials are characterized by an electron concentration typically in excess of 10^{17} cm^{-3}, leading to a plasma edge cutoff at wavelengths of about 100 μm. Magneto-transmission experiments at longer wavelengths are thus possible only in samples with exceptionally low electron concentration (i.e., about 5×10^{16} cm^{-3}). For this investigation we have been fortunate in obtaining a $Hg_{1-x}Mn_xSe$ sample of excellent quality, which after appropriate annealing had a plasma cutoff sufficiently far in the FIR to permit transmission measurements up to 170 μm.

The structure of this paper is as follows. In Sec. II we outline the theory describing intraband magneto-optical transitions in a zero-gap semiconductor when exchange interaction is present. In Sec. III we describe the far-infrared magneto-transmission experiments and sample preparation. In Sec. IV we present the details of the numerical fitting procedure used in analyzing the experimental results. Finally, in Sec. V we discuss the interpretation of the experimental results, with emphasis on their temperature dependence.

II. THEORY

The description of electronic states of a diluted magnetic semiconductor in the presence of a magnetic field is obtained by introducing the spin-spin exchange interaction as an additive term in the Hamiltonian of a nonmagnetic semiconductor. We

outline this procedure below, starting with the formulation for an "ordinary" (i.e., nonmagnetic) case, and adding the exchange contribution at a later stage.

The energy-band structure for a zero-gap nonmagnetic semiconductor in the presence of a magnetic field is described by the model of Pidgeon and Brown (PB).[2] This model treats the problem of an electron in a magnetic field in the effective-mass approximation, taking into account the contributions of the neighboring Γ_6, Γ_7, and Γ_8 bands exactly, and treating the remaining "higher" bands in an approximate way. This formulation leads to an 8×8 matrix eigenvalue problem, with the following parameters: $E_0 = E(\Gamma_6) - E(\Gamma_8)$, the interaction energy gap at the Γ point, $P = -(i\hbar/m)\langle S \mid p_z \mid Z\rangle$, the momentum matrix element, $\Delta = E(\Gamma_8) - E(\Gamma_7)$, the spin-orbit splitting at the Γ point, and γ_1, γ_2, γ_3, κ, and F—the "higher band" parameters obtained in a perturbative way with the accuracy to terms of the order of k^2, where k is the electron wave vector.

Since in the present case our interest is in the conduction electrons in zero-gap $Hg_{1-x}Mn_xSe$ (Γ_8 band), we can make the following further simplifications: Assuming the Γ_8 bands to be spherically symmetric, we can take $\gamma_2 = \gamma_3 \equiv \bar{\gamma}$. Also, since the F parameter affects only the Γ_6 band,[2] in our analysis of the Γ_8 electron states we can set $F = 0$.

For $k_z = 0$, the 8×8 matrix can be separated into two 4×4 matrices $[D_a^{\rm PB}]_{4\times 4}$ and $[D_b^{\rm PB}]_{4\times 4}$ as follows:

$$[H^{\rm PB}]_{8\times 8} = \begin{bmatrix} [D_a^{\rm PB}]_{4\times 4} & 0_{4\times 4} \\ 0_{4\times 4} & [D_b^{\rm PB}]_{4\times 4} \end{bmatrix}, \tag{1}$$

where the a and b labels correspond to the "quasi-spin-up" and "quasi-spin-down" states, respectively. From the diagonalization of these 4×4 matrices, one obtains the energies at the bottom of each Landau level ($k_z = 0$) at a given magnetic field. The observed intraband FIR absorption is dominated by transitions between these energies because the density of states has a singularity at $k_z = 0$.

As pointed out earlier, the properties of diluted magnetic semiconductors are also strongly affected by the spin-spin exchange interaction between the band electrons and the $3d$ electrons of the localized Mn^{2+} ions. The effect of this interaction on electronic states is taken into account by adding to the nonmagnetic Pidgeon-Brown Hamiltonian an exchange term[3,4] of the form

$$H_{\rm ex} = \sum_{R_i} J(\vec{r} - \vec{R}_i)\vec{S}_i \cdot \vec{\sigma}\ , \tag{2}$$

where $\vec{S}_i$ and $\vec{\sigma}$ are the spin operators of the ith Mn^{2+} ion and of the band electron, respectively, J is the electron-ion exchange coupling constant, and $\vec{r}$ and $\vec{R}_i$ are the band electron and Mn^{2+} coordinates, respectively. The summation is over all lattice sites occupied by the Mn^{2+} ions.

Two important simplifications can be made in $H_{\rm ex}$. Firstly, since the electronic wave function is very extended, so that the electron "sees" a large number of Mn^{2+} ions at any time, we may replace $\vec{S}_i$ by the thermal average $\langle \vec{S}\rangle$ of the Mn^{2+} spin, taken over all ions. We are then using the molecular field approximation. For paramagnetic systems, if the applied field $\vec{H}$ is in the z direction, $\langle \vec{S}\rangle = \langle \vec{S}_z\rangle$, a quantity intimately related to the magnetization of the system.

Secondly, and again because the electronic wave function spans a large number of lattice sites, we can replace $J(\vec{r} - \vec{R}_i)$ by $xJ(\vec{r} - \vec{R})$, where $\vec{R}$ denotes the coordinate of every site of the Mn-Hg fcc sublattice and x is the Mn concentration (mole fraction), with the summation now carried out over all $\vec{R}$. We are thereby treating the exchange interaction in terms of the virtual crystal approximation. We then have

$$H_{\rm ex} = x\sigma_z\langle S_z\rangle \sum_{\vec{R}} J(\vec{r} - \vec{R})\ . \tag{3}$$

The advantage of Eq. (3) is that it has the periodicity of the lattice, and is thus tractable within the framework of Bloch solutions, enabling the solutions of the total Hamiltonian H [which includes Eq. (3)] to be expressed in terms of the same basis functions as those of $H^{\rm PB}$, Eq. (1).

Using the basis functions of the Pidgeon-Brown model, one then obtains the additional 4×4 a and b matrices representing the exchange contribution, in the form[4]:

$$D_a^{\rm ex} = \begin{bmatrix} \frac{1}{2}N_s\alpha\langle S_z\rangle & 0 & 0 & 0 \\ 0 & \frac{1}{2}N_s\beta\langle S_z\rangle & 0 & 0 \\ 0 & 0 & -\frac{1}{6}N_s\beta\langle S_z\rangle & -i\frac{\sqrt{2}}{3}N_s\beta\langle S_z\rangle \\ 0 & 0 & i\frac{\sqrt{2}}{3}N_s\beta\langle S_z\rangle & \frac{1}{6}N_s\beta\langle S_z\rangle \end{bmatrix}, \tag{4}$$

$$D_b^{\text{ex}}=\begin{pmatrix} -\frac{1}{2}N_s\alpha\langle S_z\rangle & 0 & 0 & 0 \\ 0 & \frac{1}{6}N_s\beta\langle S_z\rangle & 0 & i\frac{\sqrt{2}}{3}N_s\beta\langle S_z\rangle \\ 0 & 0 & -\frac{1}{2}N_s\beta\langle S_z\rangle & 0 \\ 0 & -i\frac{\sqrt{2}}{3}N_s\beta\langle S_z\rangle & 0 & \frac{1}{6}N_s\beta\langle S_z\rangle \end{pmatrix} . \tag{5}$$

Here $\alpha=\langle S\,|\,J\,|\,S\rangle$ and $\beta=\langle X\,|\,J\,|\,X\rangle$ are exchange integrals corresponding to the Γ_6 and Γ_8 bands, respectively, and $N_s=xN_0$, where x is the Mn concentration and N_0 is the number of unit cells per unit volume.

Assuming the material to be paramagnetic, the average value of the spin $\langle S_z\rangle$ can be written as[5]

$$\langle S_z\rangle=-S_0B_s(x)\ , \tag{6}$$

where S_0 is the saturation spin value of Mn (treated as an adjustable parameter), and $B_s(x)$ is a modified Brillouin function given by

$$B_s(x)=\frac{2S+1}{2S}\coth\left[\frac{2S+1}{2S}x\right]-\frac{1}{2S}\coth\left[\frac{1}{2S}x\right], \tag{7}$$

where $S=\frac{5}{2}$ and

$$x=\frac{g\mu_BSB}{k_B(T+T_0)}\ .$$

Here g is the g factor of manganese (taken equal to 2),[6] μ_B is the Bohr magneton, T is the temperature, and T_0 is an adjustable temperature parameter introduced in Ref. 5. The above quantity $\langle S_z\rangle$, which determines the exchange interaction, is of course related to the magnetization M of the material by

$$M=-N_sg\mu_B\langle S_z\rangle\ . \tag{8}$$

The full Hamiltonian, containing the Pidgeon-Brown treatment of the bands and the exchange contribution, can now be written as two sets of 4×4 matrices,

$$D_a=D_a^{\text{PB}}+D_a^{\text{ex}}\ , \tag{9a}$$

$$D_b=D_b^{\text{PB}}+D_b^{\text{ex}}\ . \tag{9b}$$

By diagonalizing these matrices, one then finds the energies of the Landau levels at a given magnetic field.

Within the framework of this model there are three allowed transitions between the Landau levels which can be observed in the FIR region:

(a) cyclotron resonance, elicited by the cyclotron-resonance-active (CRA) circular polarization. Designating the nth Landau level corresponding to the D_a matrix (quasi-spin-up states) and the D_b matrix (quasi-spin-down states) by $a(n)$ and $b(n)$, respectively, the cyclotron resonance corresponds to the transitions $a(n)\rightarrow a(n+1)$ or $b(n)\rightarrow b(n+1)$, i.e., to inter-Landau-level transitions without spin flip.

(b) electric-dipole-excited spin resonance (EDSR), elicited by the cyclotron-resonance-inactive (CRI) circular polarization when the effective g factor of the conduction electrons is negative (as is the case in zero-gap semiconductors). This resonance corresponds to the $a(n)\rightarrow b(n)$ transition, i.e., it is an *intra*-Landau-level spin-flip transition.

(c) combined resonance, observed in the so-called ordinary Voigt (or parallel Voigt) geometry, i.e., excited by linearly polarized waves with $\vec{E}\|\vec{B}$. This resonance corresponds to $a(n)\rightarrow b(n+1)$, i.e., it is in an *inter*-Landau-level spin-flip transition.

The cyclotron resonance is the only electric-dipole transition allowed in a noninteracting isotropic single electron band. The two other electric-dipole transitions mentioned above (EDSR and combined resonance) become allowed in the presence of spin-orbit coupling, when the selection rules which normally forbid these transitions are relaxed as a result of wave-function mixing through the $\vec{k}\cdot\vec{p}$ interaction and/or inversion asymmetry.[7,8]

III. EXPERIMENTAL PROCEDURE AND RESULTS

The $Hg_{1-x}Mn_xSe$ crystal used in this investigation was grown by the Bridgman method. The samples were cut from the ingot using a wire saw and were annealed in dynamic vacuum at 180 °C. The composition of the samples, obtained from the density of the specimens, was $x=0.032$. Prior to the FIR transmission measurements the samples were etched in 10–15 % bromine-methanol solu-

tion to a final thickness of about 30 μm.

The measurements were carried out in magnetic fields up to 2.5 tesla using a conventional electromagnet. The source of the FIR radiation was an optically pumped FIR laser, operating at 96.5, 103, 119, 163, and 170 μm. Further details about the experimental procedure are described elsewhere.[8] The transmitted FIR signal was detected using a carbon bolometer. A lock-in amplifier with a 16-Hz chopper and an X-Y plotter were used to amplify and record the signal. The measurements were carried out in the parallel Voigt and in the Faraday geometries, the latter employing both circular polarizations. Temperatures below 4.2 K were determined from the helium vapor pressure. This also allowed us to calibrate the carbon resistor, which was then used as a thermometer for temperatures between 4.2 and 8 K.

Initial measurements on $Hg_{1-x}Mn_xSe$ ($x=0.032$) were carried out on a sample which had been annealed for 24 h. The measurements were performed at 96.5 μm at three temperatures and at 103 μm at 4.2 K. The sample was opaque at longer wavelengths, with the plasma frequency estimated at $\omega_p = 1.8\times10^{13}$ rad/s, corresponding to a cut-off wavelength of ca. 100 μm.

We then reannealed the sample for an additional 48-h period to further reduce the electron concentration. Measurements carried out directly after reannealing indicated a lower plasma frequency, estimated at $\omega_p = 1.2\times10^{13}$ rad/s, corresponding to the wavelength of 150 μm, making it possible to perform magnetotransmission experiments up to 170 μm. Measurements on the reannealed material were made at eleven temperatures between 1.9 and 6.5 K. Examples of typical magnetotransmission spectra taken in both the Faraday and the Voigt ($\vec{E}||\vec{B}$) geometries are shown in Figs. 1 and 2. The lines marked EDSR in Fig. 1 are identified as the electric dipole spin resonances. The absorption line in the Voigt data in Fig. 2 is identified as the combined resonance. Because of the fact that the dielectric constant is negative over a broad region in the vicinity of cyclotron resonance,[8,9] the data for the CRA polarization do not show a cyclotron resonance line, but rather a broad cut-off band. The analysis of this type of cyclotron absorption requires the use of the full form of the dielectric function, which is not available in analytic form. We shall not consider this here, but will focus on the spin-flip transitions.

For the CRI polarization the dielectric constant is positive in our parameter range (except possibly

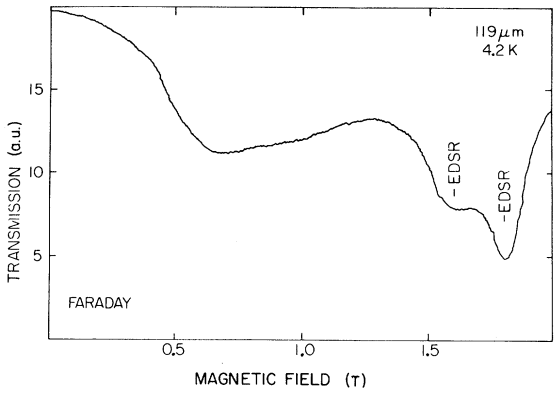

FIG. 1. Typical FIR magnetotransmission spectrum obtained on $Hg_{1-x}Mn_xSe$ in the Faraday configuration. The data was taken at 4.2 K at 119 μm wavelength, using incident linear polarization. Two electric-dipole spin resonance lines (marked EDSR in the figure) are clearly seen. The lines originate from the two lowest Landau levels. The difference in the position of the two lines is ascribed to nonparabolicity.

right at the spin-flip resonances),[8] and one can observe resolved EDSR absorption dips due to these transitions. The data for the Faraday geometry in Fig. 1 are an example of this behavior. The transmission step appearing at about 0.7 T is connected with the CRA cyclotron cut-off. The transmission at higher magnetic field is only for the CRI-polarized FIR and the dips observed, at about 1.7 T, correspond to spin-flip transitions.

Figure 2 is an illustration of the temperature

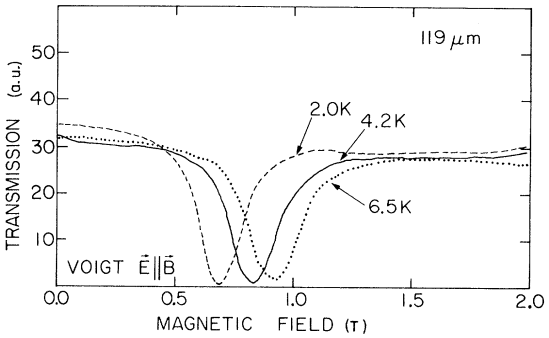

FIG. 2. Magnetotransmission spectra for the Voigt $\vec{E}||\vec{B}$ configuration obtained at 119 μm, showing the combined resonance absorption at three different temperatures, as indicated in the figure. The resonance shifts with temperature as a consequence of the temperature dependence of the exchange interaction.

behavior of the observed spin-flip resonances. The three transmission curves in Fig. 2 were taken in the Voigt ($\vec{E}||\vec{B}$) geometry at three temperatures, and correspond to the combined resonance. The temperature shift of the resonance, ascribed to the exchange interaction involving the temperature-dependent $\langle S_z \rangle$, is clearly evident.

IV. THEORETICAL FITS

The magnetic field positions of the combined and the EDSR resonances observed at 4.2 K at the five FIR wavelengths are shown in Fig. 3 as points and triangles. We have analyzed this data in terms of the modified Pidgeon-Brown model, using a numerical fitting procedure. As pointed out earlier, the quantities employed in the model are the band parameters E_0, P, Δ, $\bar{\gamma}$, γ_1, and κ, and the magnetic parameters α, β, S_0, and T_0. It is, of course, advantageous to restrict the number of fitting parameters in order to reduce the fitting error to meaningful margins. Thus we have made the reasonable assumption that the value of the spin-orbit splitting parameter Δ and the higher band parameters γ and κ are, for such low manganese concentrations ($x=0.032$), very nearly equal to those for pure HgSe. We have therefore adopted in our calculations the following HgSe parameters from the literature[8,10]: $\Delta=387$ meV, $\gamma_1=0.1$, $\bar{\gamma}=0.2$, and $\kappa=-0.7$. Of the band parameters, we will thus only be determining the energy gap E_0 and the matrix element P by fitting the data.

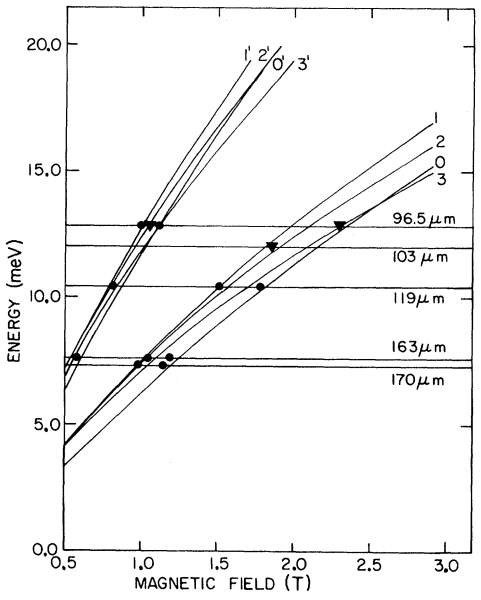

FIG. 3. Transition energies vs magnetic field for EDSR and for the combined resonance at 4.2 K. Solid dots indicate experimental data obtained at 4.2 K on the $Hg_{1-x}Mn_xSe$ specimen after final annealing. We have also shown data obtained after partial annealing (24 h, see text) corresponding to a somewhat higher plasma frequency and Fermi energy (triangles). The solid curves are calculated, representing best fits to the experimental data. The curves labeled with unprimed integers n correspond to EDSR, n denoting the initial Landau-level quantum numbers in the $a(n)\rightarrow b(n)$ transition; the primed integers n' refer to the combined resonance transition $a(n')\rightarrow b(n'+1)$. Horizontal lines indicate the energies of the laser lines used in the experiments.

Our data were taken in fields up to 2.5 T. In this range the magnetization manifests a nearly linear dependence on magnetic field. Under these conditions it is not possible to fit all four "magnetic" parameters (α, β, S_0, and T_0) appearing in Eqs. (4)–(7). We have therefore decided to fit only T_0, taking the values of α and β from Ref. 11 and assuming $S_0=\frac{5}{2}$ (the true manganese spin).

To begin the data analysis, one needs to know approximately the value of the Fermi energy E_F in order to determine between which Landau levels the transitions can take place. To estimate a starting value of E_F we first obtained an approximate value of the quantity N/m^* (where N is the free carrier concentration and m^* is the effective mass at the Fermi level) from the plasma frequency ω_p, given by

$$\omega_p=\frac{Ne^2}{\epsilon_0\kappa(\omega_p)m^*}\ , \tag{10}$$

where e is the electron charge, ϵ_0 is the vacuum permittivity, and $\kappa(\omega_p)$ is the real part of the dielectric function at ω_p, without any free-carrier contribution. Using the value of $\kappa(\omega_p)$ estimated for HgSe,[12] one can then find from the observed plasma frequency an experimental value of N/m^*. We then determine the relationship between N/m^* and the Fermi energy using the Kane band-structure model[13] and values of E_0 and P estimated for $Hg_{1-x}Mn_xSe$, for $x=0.03$, from Dobrowolska *et al.*[14] With the relationship of E_F and N/m^* so established, and the value of N/m^* obtained from the plasma frequency, we then obtain an approximate value of E_F. The above values of E_0 and P, obtained from Ref. 14, together with T_0 estimated from the $Hg_{1-x}Mn_x$ Te data of Bastard *et al.*[4] can also be used to make a plot of Landau levels like that shown in Fig. 4. With the Landau levels and the Fermi level approximately established, we can now find which transitions are possible at particu-

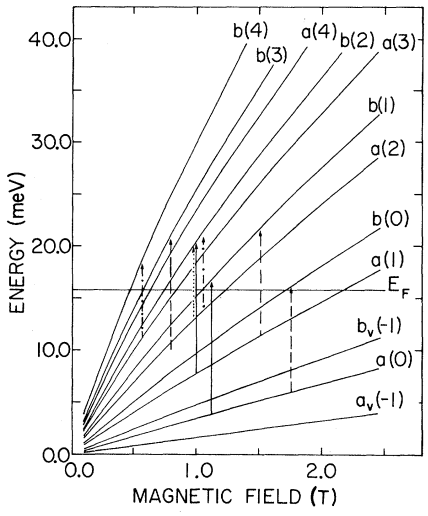

FIG. 4. Magnetic field dependence of Landau-level energies at $k_z=0$. Each Landau level is identified in the notation used in the text; $b_v(-1)$ and $a_v(-1)$ are the two uppermost Landau levels of the valence band. Note that $b_v(-1)$ lies above the lowest Landau level of the conduction band, $a(0)$. The arrows indicate observed transitions for the following laser lines: solid lines, 96.5 μm (12.84 meV); dashed lines, 119 μm (10.43 meV); dot-dashed lines, 163 μm (7.60 meV); dotted line, 170 μm (7.39 meV). The horizontal line marked E_F shows the highest possible Fermi level which allows these transitions to take place.

lar FIR wavelengths. Using that as a point of departure, we then apply the minimalization procedure to fit the theoretical positions of resonances given by the modified PB model to our data. As mentioned earlier, only E_0, P, and T_0 were treated as fitting parameters in this procedure.

Using the parameters obtained by the fitting analysis, we plot in Fig. 3 the energies of the observed resonances as a function of magnetic field. One can distinguish two groups of transitions. At the higher energies are combined resonances, corresponding to the transition $a(n')\rightarrow b(n'+1)$, with the particular values of n' for each curve indicated by primed integers. The group of lines at lower energies represents electric dipole spin resonances, corresponding to the $a(n)\rightarrow b(n)$ transitions, with n indicated by unprimed integers in the graph.

Having determined E_0 and P at 4.2 K, and assuming them to be constant with temperature, we then fit the data obtained at other temperatures (shown by points in Fig. 5). In order to fit the data, we must allow T_0 to be a function of temperature. The fits, obtained for all wavelengths with the same $T_0(T)$, are shown by continuous curves in Fig. 5. The values of T_0 versus temperature obtained in this manner are shown in Fig. 6. Using these values of T_0 and S_0, we can now also calculate the magnetic susceptibility $\chi=M/H$. The plot of χ so obtained as a function of temperature is shown in Fig. 7, and compared with susceptibilities obtained by other means. We note in passing that, in analyzing their measurements of dc magnetization in terms of Eq. (7), other workers also found that T_0 is a temperature-dependent parameter.[15]

V. DISCUSSION

From the fitting of the 4.2-K data we have obtained $E_0=-83.1$ meV, $P=5.58\times10^{-8}$ eV cm, and $T_0=7.23$ K. Our value of E_0 is in good agreement with that previously reported by Dobrowolska *et al.*[14] and by Takeyama and Galazka[16] but appears to conform better to Ref. 14. The value of P shows once again that the matrix element for diluted magnetic semiconductors is smaller than that for the related nonmagnetic zero-gap crystals (e.g., $P=7.0\times10^{-8}$ eV cm for HgSe, see Ref. 8).

We cannot explain the origin of two resonances appearing at fields about 1.3 T for 163 and 170 μm in Fig. 3 and indicated by crosses in Fig. 5. They lie near the field at which EDSR for the lowest ($n=0$) Landau level is expected, but that transition cannot occur for the present estimate of the Fermi level (see Fig. 4). If the Fermi level is lowered sufficiently to allow this transition, then our value of the plasma frequency requires the corresponding value of the low-frequency dielectric constant $\epsilon(\omega_p)$ to be at most 16, which is unreasonably small[12] [recall Eq. (10) and subsequent discussion]. It is interesting, however, that the temperature behavior of these resonances appears to parallel that of the identified EDSR lines [Figs. 5(c) and 5(d)]. The transitions marked by crosses may perhaps be associated with impurity levels, but there is at this time neither sufficient data nor theoretical understanding to warrant further discussion of these two sets of absorption lines.

One of the most striking aspects of diluted magnetic semiconductors is the strong dependence of magneto-optical resonances on temperature, as clearly evidenced by Figs. 2 and 5. For the EDSR, the resonance field shifts by about 50% between 2 and 6.5 K. The combined resonance fields are less temperature dependent, changing by about 20% be-

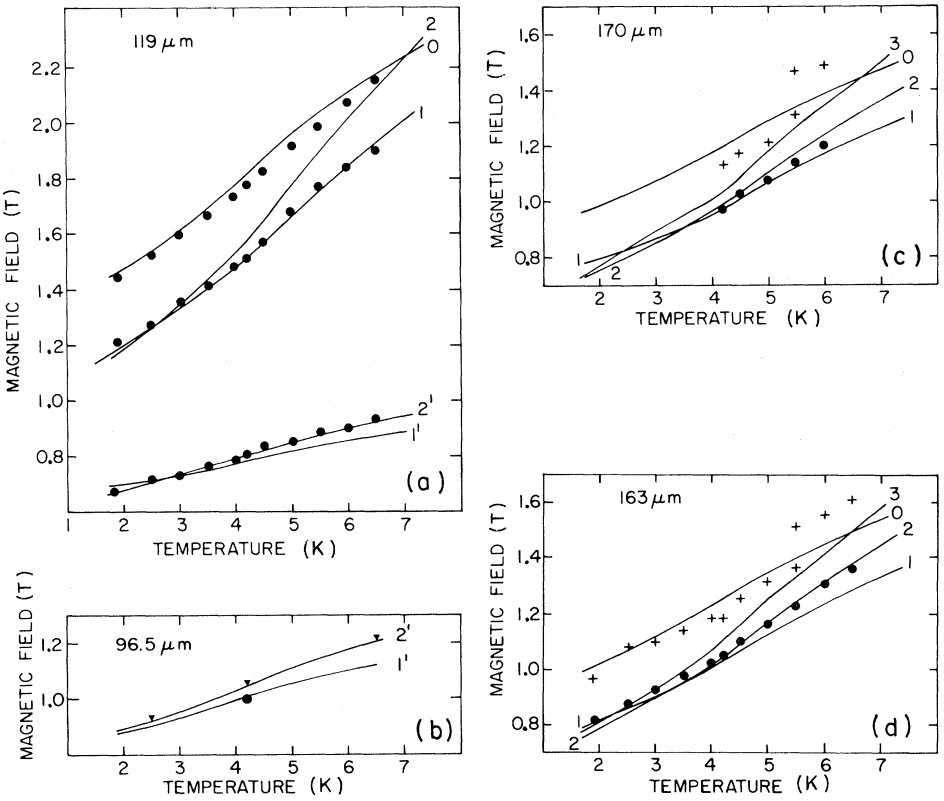

FIG. 5. Temperature dependence of resonance positions for several laser wavelengths. The points and crosses represent experimental data obtained after final annealing; the triangles are data obtained after partial annealing, as in Fig. 3. For discussion of data marked by crosses, see Sec. V. The solid curves are theoretical, using the band parameters corresponding to the fit shown in Fig. 3 and the temperature dependence of T_0 given in Fig. 6. Unprimed integers refer to EDSR, primed to the combined resonance.

tween these two temperatures. The solid lines in Fig. 5 show the theoretically predicted temperature behavior of the resonance field positions calculated using $T_0(T)$ given in Fig. 6. The fits are reasonably satisfactory, especially since they are all ob-

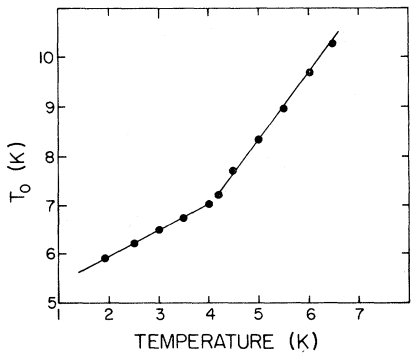

FIG. 6. Temperature dependence of the parameter T_0. The dots represent values obtained from fitting the data at a series of temperatures, as shown in Fig. 5. The solid lines are simply a guide for the eyes.

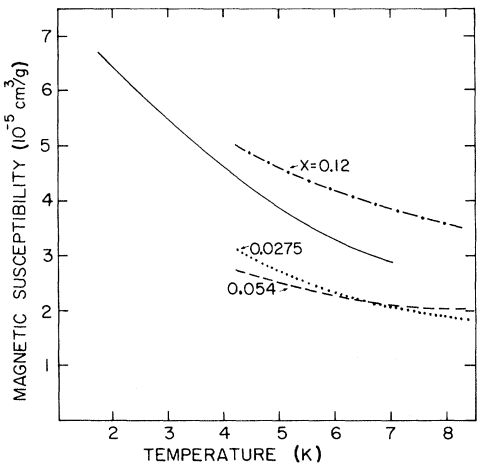

FIG. 7. Magnetic susceptibility as a function of temperature. The solid line represents our values obtained via Eqs. (6)–(8), using the temperature dependence of T_0 given in Fig. 6. The remaining curves are the values of the dc magnetic susceptibility taken from Ref. 17, and corresponding to the compositions of $Hg_{1-x}Mn_xSe$ as marked in the figure.

tained with a single set of parameters.

To demonstrate the temperature dependence of Landau levels at the Γ point, we have plotted in Fig. 8 the energies of the first three levels at two temperatures, 1.9 and 6.0 K. Level $a(1)$ is the least affected by the temperature, and level $b(0)$ is affected the most. In general, all the $b(n)$ levels (quasi-spin-down) are shifted to lower energies when the temperature is increased and are affected more than the $a(n)$ (quasi-spin-up) levels. Levels $a(0)$ and $a(1)$ also shift downward when the temperature is raised, but the energy shift is smaller; and the $a(2)$ level shifts to higher energies at higher temperatures. This behavior of the levels with temperature explains the changes of the resonance positions [see broken arrows in Fig. 8, corresponding to the $a(0)\rightarrow b(0)$ transition for 119 μm]. Figure 8 shows that, because of the value of

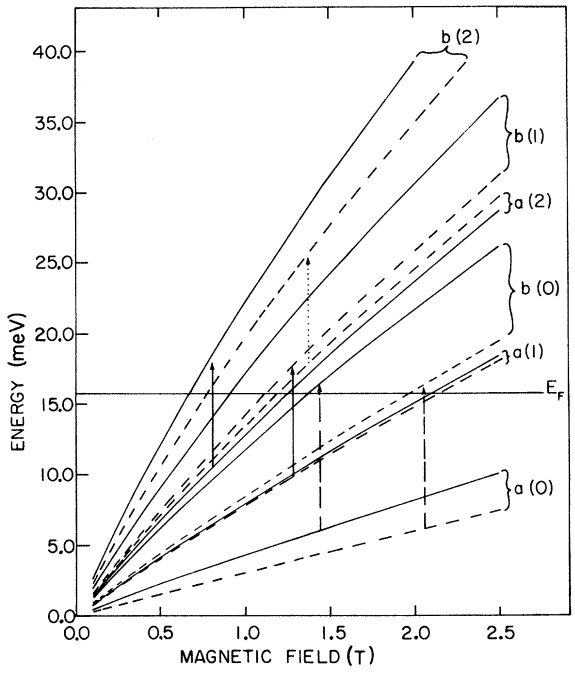

FIG. 8. Magnetic field dependence of Landau-level energies at the Γ point calculated for 1.9 K (solid lines) and 6.0 K (dashed lines) using the band parameters established in fitting Fig. 3 and the values of T_0 taken from Fig. 6. The broken arrows show how the magnetic field position of the EDSR transitions for 119 μm (10.4 meV) shifts between 1.9 and 6.0 K. The solid and dotted arrows show the EDSR transitions for 163 μm (7.6 meV). At 1.9 K, the $a(2)\rightarrow b(2)$ transition occurs at 7.6 meV, ca. 0.8 T. However, because of the values of E_F, the same transition cannot take place at 6 K (dotted arrow), and the $a(1)\rightarrow b(1)$ transition occurs instead.

the Fermi level, the resonance for 163 μm must transform from the transition $a(2)\rightarrow b(2)$ at 1.9 K to $a(1)\rightarrow b(1)$ at 6.0 K, since the initial state $a(2)$ of the former transition lies above the Fermi level at higher temperatures. In principle, at a certain intermediate temperature both transitions should be taking place simultaneously, but their positions at these temperatures (ca. 4.5 K) are so close [Fig. 5(c)] that it is impossible to observe the process of transformation of one resonance into the other.

Figure 8 can serve to illustrate yet another characteristic of diluted magnetic semiconductors. Note that although in zero-gap semiconductors without magnetic ions the cyclotron splitting is always greater than the spin splitting, in the case of zero-gap diluted magnetic semiconductors the opposite can also be true, as is clearly seen by comparing, e.g., the separation $b(0)-a(0)$ with $a(1)-a(0)$ in Fig. 8. Furthermore, in nonmagnetic semiconductors the largest spin splitting corresponds to the lowest Landau level ($n=0$), but in our case again the situation is different. In the investigated magnetic field region even the third ($n=2$) Landau level has a larger spin splitting than the first ($n=0$). Similar new features can be seen in the case of the combined resonance (see Fig. 3).

Finally, using the Landau-level structure calculated with the parameters obtained by fitting the experimental data, we can also calculate the cyclotron resonance fields for a given laser line at different temperatures. The results, shown in Fig. 9, are somewhat unexpected: They indicate temperature shifts in the cyclotron resonance fields that are as large as for the EDSR. This effect, especially pronounced for the transition $a(0)\rightarrow a(1)$, is a consequence of the fact that successive Landau levels are affected *differently* by the exchange interaction: e.g., since—as illustrated in Fig. 8—the level $a(0)$ is affected to a different degree than $a(1)$, the transition $a(0)\rightarrow a(1)$ will shift in energy as the magnetization changes with temperature. As shown in Fig. 9, the predicted temperature shift of the cyclotron resonance position is opposite in direction to that of the spin-flip resonances (Fig. 5). The shift is less dramatic for the $b(0)\rightarrow b(1)$ transitions (lower part of Fig. 9), but still shows the properties described.

By knowing the magnetization parameters S_0 and T_0 and the manganese concentration x, we can calculate the magnetic susceptibility, as described in Sec. II. The dependence of the susceptibility obtained in this manner on temperature is shown in

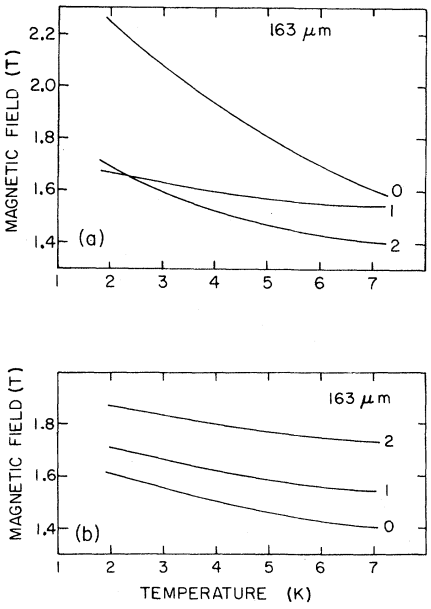

FIG. 9. Temperature dependence of the positions of cyclotron resonances calculated for 163 μm using the band parameters obtained from fitting Fig. 3 and $T_0(T)$ given in Fig. 6. The upper set of curves correspond to transitions $a(n) \rightarrow a(n+1)$, with n as marked; the lower frame corresponds to transitions $b(n) \rightarrow b(n+1)$.

Fig. 7. For comparison we have plotted in the same figure the measured dc susceptibility[17] for $x = 0.0275$, 0.054, and 0.12. Our curve lies above the curves for $x = 0.0275$ and 0.054 but below that for $x = 0.12$ and shows about the same temperature dependence as the $x = 0.0275$ sample. The deviation of about 25% between the data for $x = 0.0275$ and our data is rather satisfactory, considering the difference in the methods of obtaining the values of the susceptibility. This corroborates the conclusion that the temperature dependence of the spin splitting between 2 and 6.5 K, inferred from the spin-flip resonances, is completely determined by the temperature dependence of the magnetization.

ACKNOWLEDGMENTS

The authors wish to thank M. Jaczynski for preparation of the $Hg_{1-x}Mn_xSe$ samples, and M. Dobrowolska and D. D. Kirchhofer for valuable discussions. The support of the NSF Grant No. DMR 79-23310 and the Purdue Central Laser Facility operated under NSF-MRL Grant No. DMR 80-20249 is gratefully acknowledged.

*Permanent address: Institute of Experimental Physics, Warsaw University, 00-681, Warsaw, Poland.

[1]See, e.g., J. A. Gaj, Proceedings of the 15th International Conference on the Physics of Semiconductors, Kyoto, 1980 [J. Phys. Soc. Jpn. 49, Suppl. A, 797 (1980)].

[2]C. R. Pidgeon and R. N. Brown, Phys. Rev. 146, 575 (1966); W. Leung and L. Liu, Phys. Rev. B 8, 3811 (1973).

[3]J. Kossut, Phys. Status Solidi B 78, 537 (1976).

[4]G. Bastard, C. Rigaux, and A. Mycielski, Phys. Status Solidi B 79, 585 (1977); G. Bastard, C. Rigaux, Y. Guldner, J. Mycielski, and A. Mycielski, J. Phys. 39, 87 (1978).

[5]J. A. Gaj, R. Planel, and G. Fishman, Solid State Commun. 29, 435 (1979).

[6]R. T. Holm and J. K. Furdyna, Solid State Commun. 15, 1459 (1974).

[7]B. D. McCombe, Phys. Rev. 181, 1206 (1969).

[8]K. Pastor, M. Jaczynski, and J. K. Furdyna, Phys. Rev. B 24, 7313 (1981).

[9]E. D. Palik and J. K. Furdyna, Rep. Prog. Phys. 33, 1193 (1970).

[10]M. Dobrowolska, W. Dobrowolski, and A. Mycielski, Solid State Commun. 34, 441 (1980).

[11]P. Byszewski, M. Z. Cieplak, and A. Mongird-Gorska, J. Phys. C 13, 5383 (1980).

[12]A. M. Witowski and M. Grynberg, Phys. Status Solidi B 100, 389 (1980).

[13]E. O. Kane, J. Phys. Chem. Solids 1, 249 (1957); E. O. Kane, in *Physics of III-V Compounds*, edited by R. K. Willardson and A. C. Beer (Academic, New York, 1966), Vol. I, p. 75.

[14]M. Dobrowolska, W. Dobrowolski, M. Otto, T. Dietl, and R. R. Galazka, Proceedings of the 15th International Conference on the Physics of Semiconductors, Kyoto, 1980 [J. Phys. Soc. Jpn. 49, Suppl. A, 815 (1980)].

[15]W. Dobrowolski, M. von Ortenberg, A. Sandauer, R. R. Galazka, and R. Pauthenet, Proceedings of the 4th International Conference on the Physics of Narrow Gap Semiconductors, Linz, 1981 (in press).

[16]S. Takeyama and R. R. Galazka, Phys. Status Solidi B 96, 413 (1979).

[17]G. D. Khattak, C. D. Amarasekara, S. Nagata, R. R. Galazka, and P. H. Keesom, Phys. Rev. B 23, 3553 (1981).